Bistable Magnetoresistance Switching in Exchange-Coupled $CoFe_2O_4$—Fe_3O_4 Binary Nanocrystal Superlattices by Self-Assembly and Thermal Annealing

Jun Chen,[†] Xingchen Ye,[‡] Soong Ju Oh,[†] James M. Kikkawa,[§] Cherie R. Kagan,[†,‡,⊥] and Christopher B. Murray[†,‡,*]

[†]Department of Materials Science and Engineering, [‡]Department of Chemistry, [§]Department of Physics and Astronomy, and [⊥]Department of Electrical and Systems Engineering, University of Pennsylvania, Philadelphia, Pennsylvania 19104, United States

ABSTRACT Self-assembly of multicomponent nanocrystal superlattices provides a modular approach to the design of metamaterials by choosing constituent nanocrystal building blocks with desired physical properties and engineering the interparticle coupling. In this work, we report the self-assembly of binary nanocrystal superlattices composed of magnetically hard $CoFe_2O_4$ nanocrystals and magnetically soft Fe_3O_4 nanocrystals. Both $NaZn_{13}$- and $MgZn_2$-type $CoFe_2O_4$—Fe_3O_4 binary nanocrystal superlattices have been formed by the liquid—air interfacial assembly approach. Exchange coupling is achieved in both types of binary superlattices after thermal annealing under vacuum at 400 °C. The exchange-coupled $CoFe_2O_4$—Fe_3O_4 binary nanocrystal superlattices show single-phase magnetization switching behavior and magnetoresistance switching behavior below 200 K. The $NaZn_{13}$-type $CoFe_2O_4$—Fe_3O_4 binary nanocrystal superlattices annealed at 500 °C even exhibit bistable magnetoresistance switching behavior at room temperature constituting a simple nonvolatile memory function.

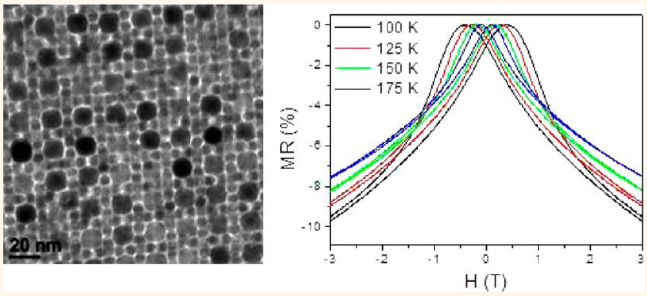

KEYWORDS: binary nanocrystal superlattices · BNSLs · self-assembly · exchange coupling · magnetoresistance · magnetic nanocrystal

Th self-assembly of nanocrystal superlattices has attracted great attention for its scientific interest and technological applications.[1,2] Nanocrystal superlattices are model systems to study collective physical and chemical properties because of the long-range periodic structure, well controlled nanocrystal positions, and interparticle distance.[3−7] Recent advances in synthetic methods allow production of highly monodisperse nanocrystals that can be integrated into large area single component nanocrystal superlattices or even binary nanocrystal superlattices (BNSLs).[8−16] Incorporating two types of nanocrystals into BNSLs can bring novel properties arising from the interaction between neighboring different functional nanocrystals. There have been extensive studies on the self-assembly and structural characterization of BNSLs, which have resulted in the discovery of more than 20 BNSL structures including a quasicrystalline phase.[17−29] However, only a few studies have investigated the collective physical properties of BNSLs.[30−33]

Exchange coupling between magnetically hard and soft materials has been widely utilized to engineer the properties of magnetic composites.[34] Exchange coupling in core/shell structured magnetic nanocrystals has also been well studied, and can be synthesized using the seed-mediated growth method with an architecture of hard magnetic core and soft magnetic shell or *vice versa*.[35−41] On the other hand, realization of magnetic exchange coupling orchestrated by the self-assembly of magnetic nanocrystals has rarely been reported. Sun and co-workers demonstrated the first example of exchange-coupled magnetic nanocomposites utilizing the self-assembly of FePt and Fe_3O_4 nanocrystals,[42] which show one-phase magnetic switching behavior and an enhanced magnetic energy

* Address correspondence to cbmurray@sas.upenn.edu.

Received for review November 12, 2012 and accepted December 30, 2012.

Published online December 30, 2012
10.1021/nn3052617

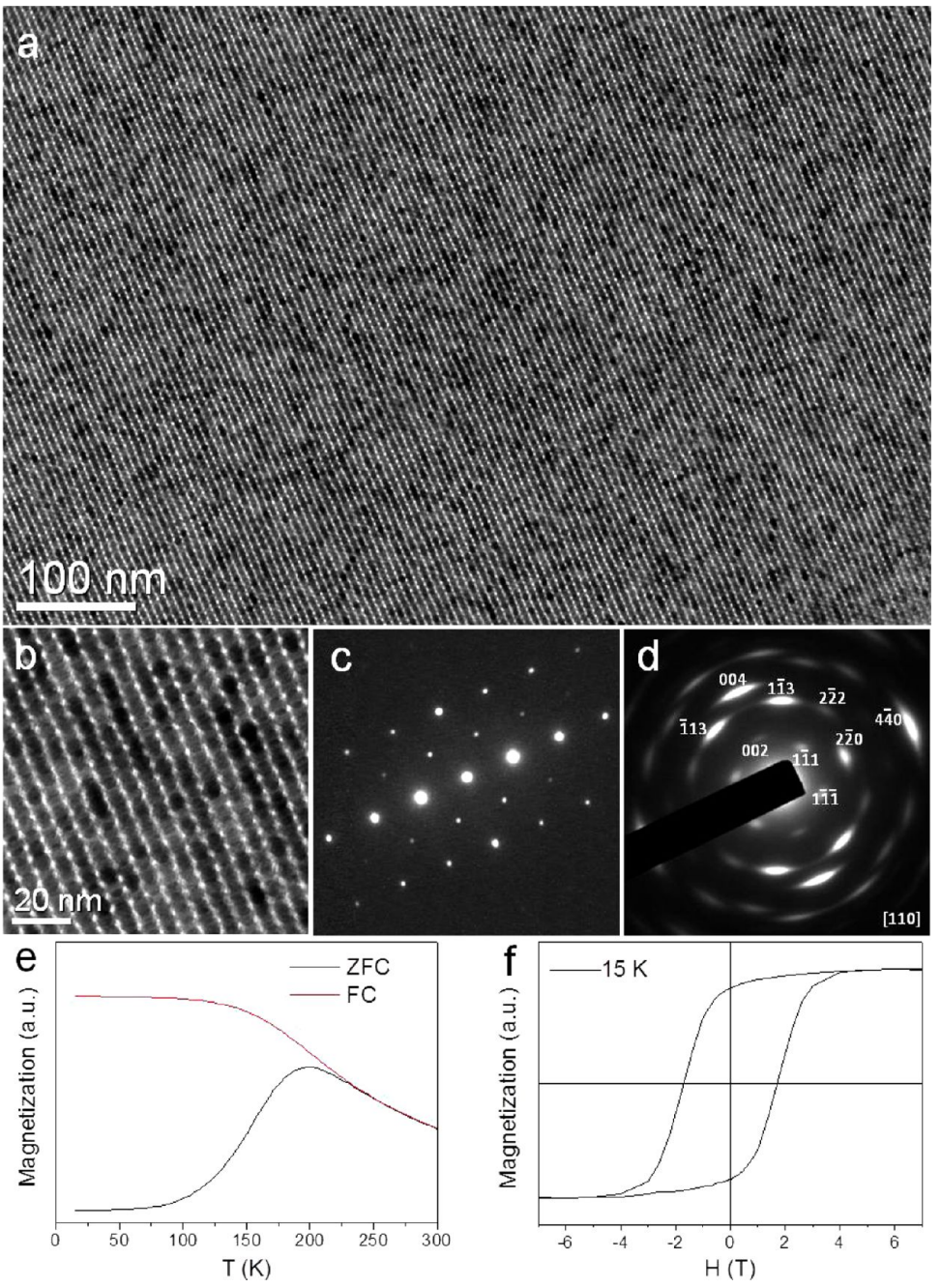

Figure 1. (a,b) Low magnification and high magnification TEM images of truncated octahedral $CoFe_2O_4$ NC superlattices, respectively; (c,d) small-angle and wide-angle ED patterns of truncated octahedral $CoFe_2O_4$ NC superlattices, respectively; (e) zero-field-cooled (ZFC) and field-cooled (FC) warming curves of truncated octahedral $CoFe_2O_4$ NC superlattices; (f) magnetization hysteresis loop of truncated octahedral $CoFe_2O_4$ superlattices at 15 K.

product due to exchange coupling. The as-synthesized FePt and Fe_3O_4 nanocrystals are both magnetically soft; therefore high temperature annealing under Ar + 5% H_2 atmosphere at 650 °C is required to convert the soft FePt and soft Fe_3O_4 binary nanocrystal assemblies into hard FePt and soft Fe_3Pt nanocomposites. In the current work, we provide another example of exchange coupling utilizing the self-assembly of $CoFe_2O_4$ and Fe_3O_4 nanocrystals into BNSLs. We choose $CoFe_2O_4$ and Fe_3O_4 nanocrystals as building blocks, because the as-synthesized $CoFe_2O_4$ and Fe_3O_4 nanocrystals are magnetically hard and soft, respectively. The pristine self-assembled $CoFe_2O_4$–Fe_3O_4 BNSLs do not show exchange coupling as they are spaced by the organic capping ligands present at the nanocrystal surface that are used in their synthesis and assembly. After thermal annealing under vacuum at 400 °C, the $CoFe_2O_4$–Fe_3O_4 BNSLs still maintain the periodic structure and become exchange coupled, showing single-phase magnetic switching and bistable magnetoresistance switching behaviors. Increasing annealing temperature to 500 °C enables the $NaZn_{13}$-type

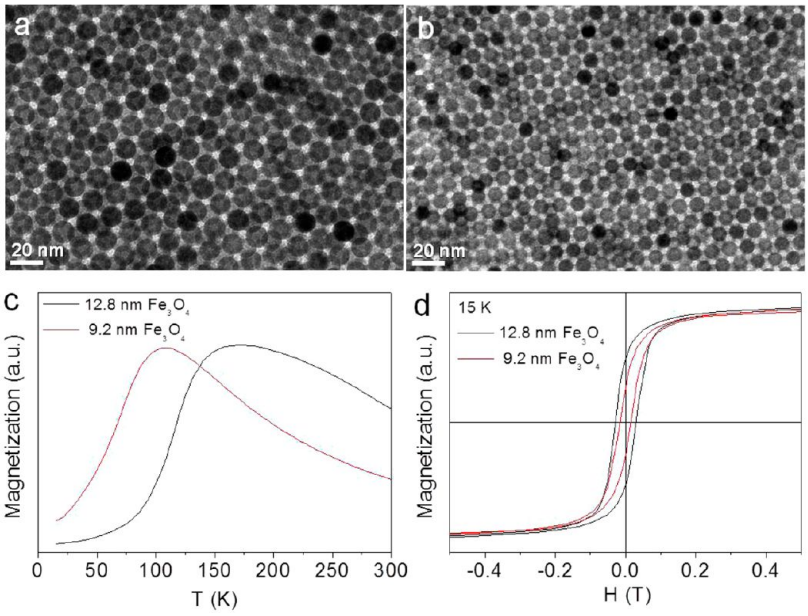

Figure 2. (a) TEM images of 12.8 nm Fe_3O_4 NCs. (b) TEM images of 9.2 nm Fe_3O_4 NCs. (c) ZFC curves of 12.8 and 9.2 nm Fe_3O_4 NCs. (d) Magnetization hysteresis loop of 12.8 and 9.2 nm Fe_3O_4 NCs at 15 K.

$CoFe_2O_4$–Fe_3O_4 BNSLs to exhibit magnetoresistance switching behavior at room temperature forming the basis of a simple nonvolatile memory element.

RESULTS AND DISCUSSION

There have been many reports on the synthesis of spinel ferrite MFe_2O_4 (M = Fe, Co, Mn, Ni, Zn, *etc.*) nanocrystals, as they represent an important class of magnetic material useful for many technological applications such as magnetic recording media and electromagnetic and spintronic devices.[11,12] In this work, the $CoFe_2O_4$ nanocrystals (NCs) were synthesized based upon the protocol first reported by Sun *et al.*,[11] in which iron(III) acetylacetonate and cobalt(II) acetylacetonate were used as precursors, oleic acid, oleylamine, and 1,2-hexadecanediol served as surfactants and reducing agents, and benzyl ether was used as the high boiling point solvent. We find the size uniformity of as-synthesized $CoFe_2O_4$ NCs can be improved by increasing the molar ratio of oleylamine to oleic acid from 1:1 to 5:1. The $CoFe_2O_4$ (6.8 nm) NCs form large area superlattices as revealed by TEM images and corresponding small-angle electron diffraction patterns as shown in Figure 1a,c. A closer view of the TEM images (Figure 1b) reveals that $CoFe_2O_4$ NCs are truncated octahedral rather than being truly spherical. The small- and wide-angle electron diffraction patterns of the $CoFe_2O_4$ NC superlattices (Figure 1c,d) show both positional and orientational ordering. To confirm whether the as-synthesized $CoFe_2O_4$ NCs are magnetically hard, we use a superconducting quantum interference device (SQUID) magnetometer to measure zero-field-cooled and field-cooled warming curves, as well as hysteresis loops at 15 K. The $CoFe_2O_4$ NCs show a blocking temperature of 197 K and coercive field of 1.7 T at 15 K (Figure 1e,f), which confirms that the $CoFe_2O_4$ NCs have high magnetocrystalline anisotropy. It is worth mentioning that the improved synthesis of monodisperse magnetically hard $CoFe_2O_4$ NCs is essential for the self-assembly of the $CoFe_2O_4$–Fe_3O_4 BNSLs.

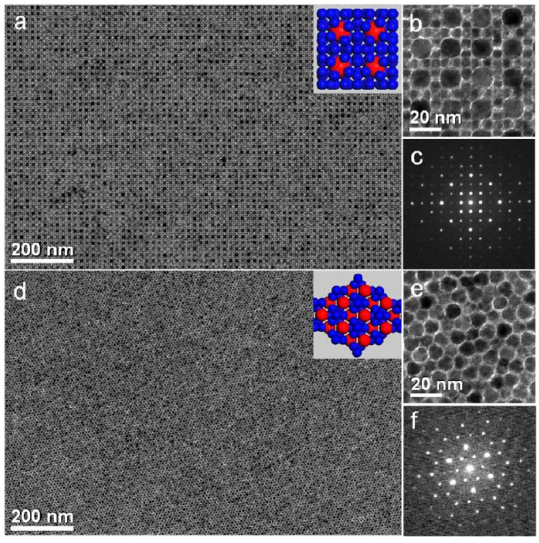

Figure 3. (a–c) Low and high magnification TEM images and small-angle electron diffraction patterns of $NaZn_{13}$-type BNSLs self-assembled from 12.8 nm Fe_3O_4 and 6.8 nm $CoFe_2O_4$ NCs. Inset is the model of $NaZn_{13}$ structure. (d–f) Low and high magnification TEM images and small-angle electron diffraction patterns of $NaZn_{13}$-type BNSLs self-assembled from 9.2 nm Fe_3O_4 and 6.8 nm $CoFe_2O_4$ NCs. Inset is the model of $MgZn_2$ structure.

The magnetically soft Fe_3O_4 NCs were synthesized using a synthetic procedure first reported by Hyeon *et al.*,[12] where iron(III) oleate was used as the precursor,

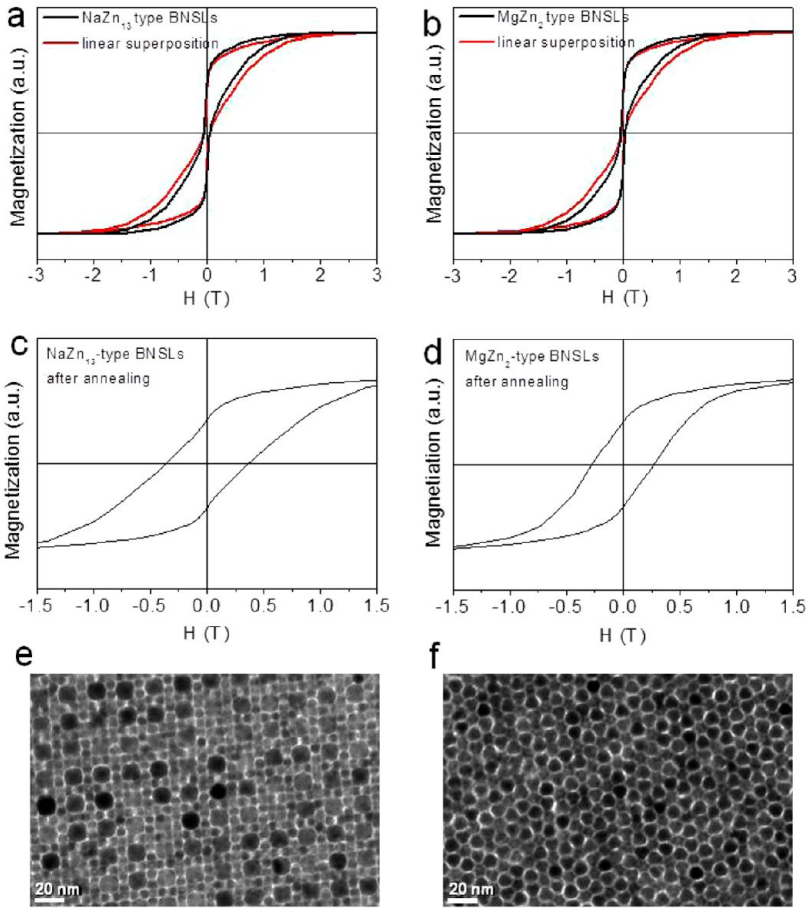

Figure 4. (a,c) Magnetization hysteresis loops of $NaZn_{13}$-type $CoFe_2O_4$–Fe_3O_4 BNSLs at 100 K before (a) and after (c) annealing at 400 °C, respectively. Red curve in panel a represents linear superposition of hysteresis loops of the individual constituent NCs. (b,d) Magnetization hysteresis loops of $MgZn_2$-type $CoFe_2O_4$–Fe_3O_4 BNSLs at 100 K before (b) and after (d) annealing at 400 °C, respectively. Red curve in panel b represents linear superposition of hysteresis loops of the individual constituent NCs. (e,f) TEM images of $NaZn_{13}$-type and $MgZn_2$-type $CoFe_2O_4$–Fe_3O_4 BNSLs after annealing at 400 °C, respectively.

oleic acid as the surfactant, and 1-octadecene as the high boiling point solvent. The size of Fe_3O_4 NCs can be adjusted by varying the reaction temperature and the molar ratio of oleic acid to iron oleate. It has been theoretically predicted that in order to obtain effective exchange coupling between the magnetically hard and soft phase, the linear domain wall width of the soft magnetic phase should not exceed twice that of the hard phase.[34] Given the size of the magnetically hard $CoFe_2O_4$ NCs (6.8 nm), we chose to explore two different sized monodisperse Fe_3O_4 NCs with diameters of 12.8 and 9.2 nm, respectively, as shown in Figure 2 panels a and b. The magnetic measurement confirms that the Fe_3O_4 NCs are magnetically soft as shown in Figure 2c,d. The 12.8 and 9.2 nm Fe_3O_4 NCs show magnetic coercive fields of 0.029 and 0.015 T at 15 K, respectively, which is nearly 2 orders of magnitude smaller than that of the 6.8 nm $CoFe_2O_4$ NCs.

The $CoFe_2O_4$–Fe_3O_4 BNSLs were self-assembled by the liquid–air interfacial assembly approach.[26] A hexane solution (15 μL) of mixed $CoFe_2O_4$ and Fe_3O_4 NCs with appropriate concentration ratios was drop cast onto the diethylene glycol surface. After the hexane was completely evaporated, the BNSL film formed on the diethylene glycol surface, and was transferred onto TEM grids for structural characterization. For the 6.8 nm $CoFe_2O_4$ and 12.8 nm Fe_3O_4 NC combination, continuous BNSLs isostructural with $NaZn_{13}$ were formed, as shown in Figure 3a–c and Supporting Information, Figure S2. In the $NaZn_{13}$ type $CoFe_2O_4$–Fe_3O_4 BNSLs, the larger Fe_3O_4 NCs form a simple cubic lattice, inside which every 13 $CoFe_2O_4$ NCs form an icosahedron surrounding each of the larger Fe_3O_4 NCs.[24] Using 9.2 nm Fe_3O_4 and 6.8 nm $CoFe_2O_4$ NCs in combination, continuous $CoFe_2O_4$–Fe_3O_4 BNSLs isostructural with $MgZn_2$ were formed, as shown in Figure 3d–f and Supporting Information, Figure S3. In the $MgZn_2$ type $CoFe_2O_4$–Fe_3O_4 BNSLs, the larger Fe_3O_4 NCs possess hexagonal diamond-like ordering, while the smaller $CoFe_2O_4$ NCs form tetrahedra surrounding the larger Fe_3O_4 NCs.[19]

Magnetic hysteresis loops of the self-assembled $NaZn_{13}$-type and $MgZn_2$-type $CoFe_2O_4$–Fe_3O_4 BNSLs measured at 100 K both show a necking character (Figure 4a,b), which indicates a two-phase magnetic switching behavior that approximates a weighted average of the hysteresis loops of the individual constituent NCs

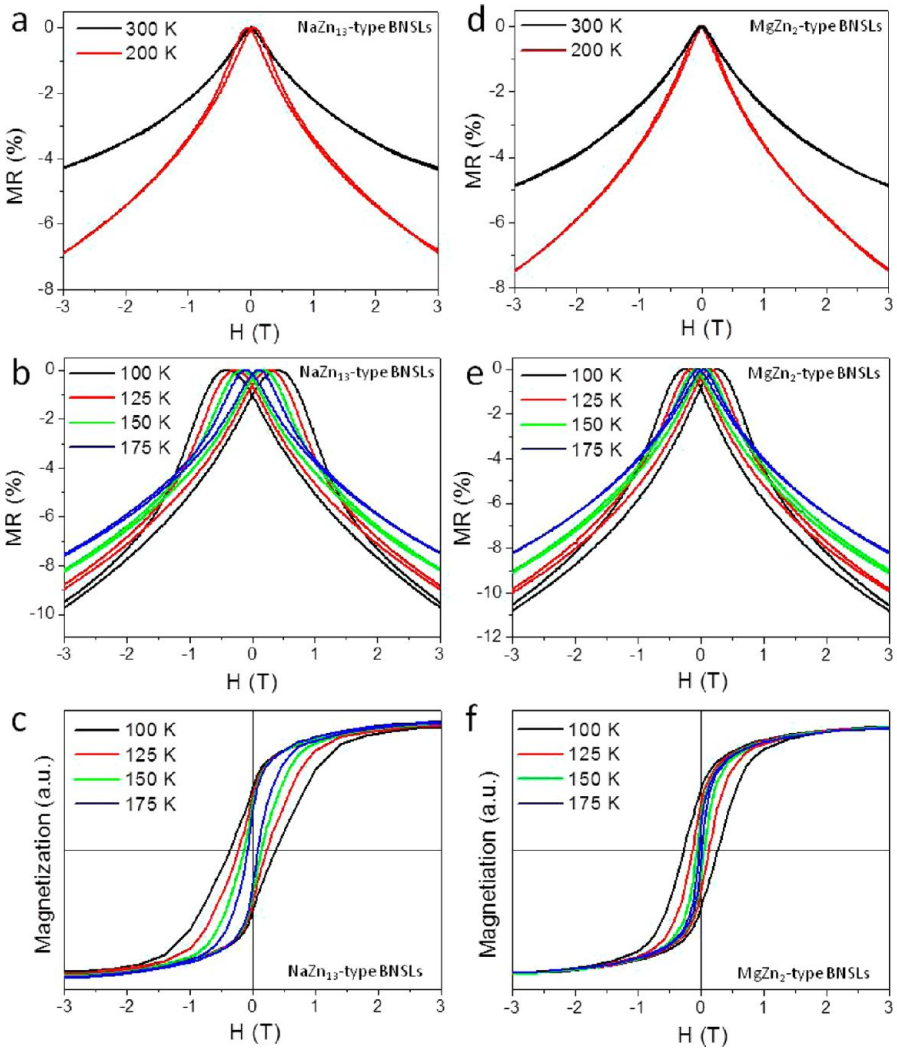

Figure 5. (a–c) Magnetoresistance curves and magnetization hysteresis loops of $NaZn_{13}$-type BNSLs composed of 12.8 nm Fe_3O_4 and 6.8 nm $CoFe_2O_4$ NCs annealed at 400 °C under vacuum. (d–f) Magnetoresistance curves and magnetization hysteresis loops of $MgZn_2$-type BNSLs composed of 9.2 nm Fe_3O_4 and 6.8 nm $CoFe_2O_4$ NCs annealed at 400 °C under vacuum.

(red curves in Figures 4a,b). The magnetically soft Fe_3O_4 phase switches at a lower magnetic field, whereas the magnetically hard $CoFe_2O_4$ phase switches at a higher magnetic field, which gives rise to the necking character of the hysteresis loops. This two-phase magnetic switching behavior suggests that there is no exchange coupling between the magnetically hard $CoFe_2O_4$ NCs and the magnetically soft Fe_3O_4 NCs. The absence of exchange coupling in the $CoFe_2O_4$–Fe_3O_4 BNSLs is expected as each NC is capped by organic ligands with long alkyl chains (oleic acid and oleylamine). To introduce exchange coupling between $CoFe_2O_4$ and Fe_3O_4 NCs, the NC surface capping organic ligands need to be removed and therefore neighboring $CoFe_2O_4$ and Fe_3O_4 NCs physically contact. Thermal annealing provides an efficient way to remove organic ligands for oxide nanocrystals.[43] We performed thermal annealing at 400 °C for 30 min under vacuum, at which the organic ligands can be completely removed, as confirmed by Fourier transform infrared spectra (FTIR) (Supporting Information, Figure S4) and thermogravimetric analysis (TGA) (Supporting Information, Figure S5). TEM images (Figure 4e,f, Supporting Information, Figures S6,S7) show that the ordering of BNSLs was preserved after thermal annealing. The magnetic hysteresis loops of the thermally annealed $NaZn_{13}$-type and $MgZn_2$-type $CoFe_2O_4$–Fe_3O_4 BNSLs measured at 100 K show a smooth change of magnetization as a function of applied magnetic field, as well as increased coercivity (Figure 4c,d). This one-phase magnetization switching behavior suggests that the $CoFe_2O_4$ and Fe_3O_4 NCs become exchange-coupled in the thermally annealed $CoFe_2O_4$–Fe_3O_4 BNSLs.[42] Furthermore, the thermally annealed $NaZn_{13}$-type $CoFe_2O_4$–Fe_3O_4 BNSLs exhibit a coercivity of 3.6 KOe at 100 K, while the $MgZn_2$-type BNSLs have a smaller coercivity of 2.7 KOe, which is presumably due to the stronger exchange coupling and higher volume ratio of the hard magnetic phase in the $NaZn_{13}$-type $CoFe_2O_4$–Fe_3O_4 BNSLs.

To study the magnetotransport properties of the exchange coupled $CoFe_2O_4$–Fe_3O_4 BNSLs, the BNSLs

self-assembled on the diethylene glycol surface were transferred to sapphire substrates with photolithographically patterned Cr/Au electrodes, followed by annealing under vacuum at 400 °C. Thermal annealing removes the insulating organic ligands and increases electronic coupling between NCs. The resistivities of the $NaZn_{13}$-type and $MgZn_2$ type BNSLs after annealing at 400 °C are 58 and 26 Ω cm, respectively. The resistivity of the thermally annealed $CoFe_2O_4$–Fe_3O_4 BNSLs increased monotonically with decreasing temperature and the zero-bias-voltage conductance (G_0) follows $T^{-1/2}$ dependence (Supporting Information, Figure S8). This temperature dependence suggests the charge transport mechanism is dominated by thermally assisted interparticle tunneling and interparticle electron hopping.[43−45] Magnetic fields were applied parallel to the BNSL films in forward and reverse directions at different temperatures. The sweep rate was 0.2 T/min for $|H| < 3$ T, and 0.5 T/min for $|H| > 3$ T. The magnetoresistance (MR) is defined as $MR = (R_H - R_{max})/R_{max}$, where R_H is the resistance at an applied magnetic field, and R_{max} is the largest resistance. Below 200 K, both the $NaZn_{13}$ and $MgZn_2$ type $CoFe_2O_4$–Fe_3O_4 BNSL films show symmetrical and hysteretic MR (Figure 5b,e). This switching behavior is different from the previously reported single-component Fe_3O_4 NC films[43−45] or Fe_3O_4–Fe_3O_4 BNSL films,[26] in which there was no MR switching even at 100 K and the maximum resistance occurred at zero magnetic field.

For the exchange coupled $CoFe_2O_4$–Fe_3O_4 BNSL films, as the magnetic field scans from −9 T to +9 T the resistance reaches a maximum value at a positive magnetic field (Figure 5, Supporting Information, Figure S9), which we call the positive MR switching field. We denote the maximum in the reverse scanning direction from +9 T to −9 T as the negative MR switching field and note that the absolute values of the positive and negative MR switching fields are almost the same. Such MR switching behavior has been observed in $CoFe_2O_4$(5 nm)/Fe_3O_4(15 nm) bilayers grown by oxygen plasma-assisted molecular-beam epitaxy,[46] in which the exchange interactions exist at the bilayer interface. Similar MR switching phenomenon has also been previously reported in metallic magnetic cobalt nanocrystal superlattices[47] and granular magnetic cobalt–copper systems at 5 K,[48] in which the magnetoresistance switching field is correlated to the magnetic coercive field and the maximum resistance occurs at the magnetic field where the global magnetization is zero. In magnetic nanocrystal arrays, the negative magnetoresistance is caused by spin-dependent tunneling; that is, the alignment of the electronic spins from neighboring nanocrystals at an applied magnetic field leads to higher tunneling probabilities and lower resistance.[43,47] By comparing the MR curves (Figure 5b,e, Supporting Information, Figure S9) to the magnetization hysteresis loops of the exchange-coupled $CoFe_2O_4$–Fe_3O_4 BNSL films measured at the same temperature (Figure 5c,f, Figure S9), we found that in the exchange-coupled $CoFe_2O_4$–Fe_3O_4 BNSL films, the MR switching field is very close to the value of the magnetic coercive field. Although it is possible to obtain hysteretic MR curves arising solely from the hysteresis of the internal field of the film, which will have contributions from the external field and the magnetization, in our case both numerical and analytic estimates show the latter self-field is too small to account for the data. The MR switching field of the exchange-coupled $CoFe_2O_4$–Fe_3O_4 BNSL films decreases as temperature increases (Figure 5b,e, Supporting Information, Figure S9), which is consistent with the trend of decreasing coercive field with increasing temperature (Figure 5c,f, Figure S9). It is also worth mentioning that the negative MR of the exchange-coupled $CoFe_2O_4$–Fe_3O_4 BNSL films does not saturate even at 9 T, whereas the magnetization is saturated at this field (Supporting Information, Figure S9). This contrast is often observed in magnetic nanocrystal arrays and can be explained by field

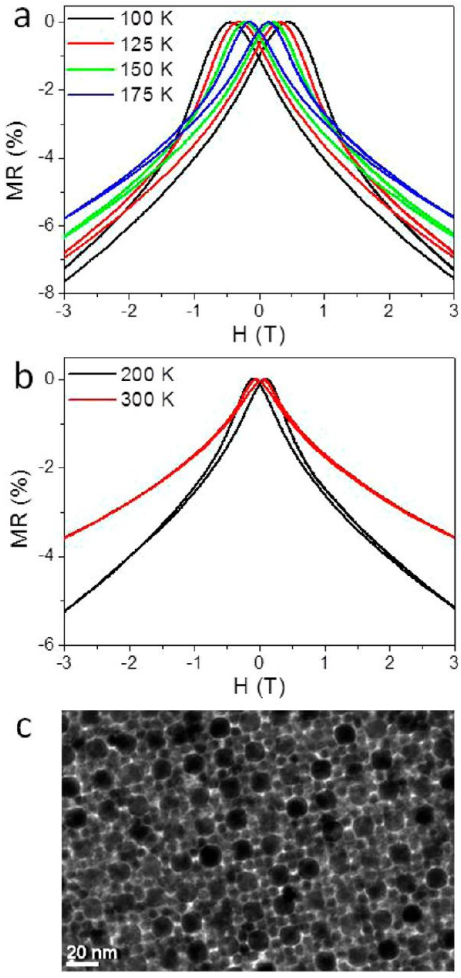

Figure 6. (a,b) Magnetoresistance curves of $NaZn_{13}$-type BNSLs composed of 12.8 nm Fe_3O_4 and 6.8 nm $CoFe_2O_4$ NCs annealed at 500 °C under vacuum. (c) TEM image of $NaZn_{13}$-type BNSLs composed of 12.8 nm Fe_3O_4 and 6.8 nm $CoFe_2O_4$ NCs annealed under vacuum at 500 °C.

dependence of spin canting at the nanocrystal surfaces.[43,44]

The magnetotransport properties of $CoFe_2O_4$–Fe_3O_4 BNSLs were further explored with higher annealing temperature of 500 °C. The TEM images (Figure 6c, Supporting Information, Figure S10) show that the ordering of the $NaZn_{13}$-type $CoFe_2O_4$–Fe_3O_4 BNSLs can still be preserved after thermal annealing under vacuum at 500 °C for 30 min. Compared to the same type of BNSLs annealed at 400 °C (Figure 5b,c), the $NaZn_{13}$-type $CoFe_2O_4$–Fe_3O_4 BNSL sample annealed at 500 °C exhibits larger magnetoresistance switching fields (Figure 6a,b), which can be ascribed to stronger exchange coupling due to closer interparticle contact after annealing at higher temperature. The $NaZn_{13}$-type $CoFe_2O_4$–Fe_3O_4 BNSLs annealed at 500 °C even exhibit magnetoresistance switching behavior at room temperature (Figure 6b). On the other hand, the $NaZn_{13}$-type $CoFe_2O_4$–Fe_3O_4 BNSLs annealed at 500 °C exhibit lower magnetoresistance values compared to the same type of BNSL sample annealed at 400 °C. The trend that magnetoresistance value decreases with increasing annealing temperature has been previously reported in magnetite nanocrystal arrays,[43,44] which was ascribed to the decreased number of surface spins that are noncollinear with the nanocrystal core at a higher annealing temperature.

CONCLUSION

In summary, monodisperse magnetically hard $CoFe_2O_4$ and soft Fe_3O_4 NCs were synthesized and used as building blocks to form BNSLs using the liquid–air interfacial assembly approach. Exchange coupling in $NaZn_{13}$- and $MgZn_2$-type $CoFe_2O_4$–Fe_3O_4 BNSLs were achieved after thermal annealing at 400 °C under vacuum. The exchange-coupled $CoFe_2O_4$–Fe_3O_4 BNSLs show one phase magnetization switching behavior and magnetoresistance switching behavior below 200 K. Increasing the annealing temperature to 500 °C enables the $NaZn_{13}$-type $CoFe_2O_4$–Fe_3O_4 BNSLs to exhibit magnetoresistance switching behavior at room temperature.

METHODS

Materials. The following chemicals were used as received. Iron(III) chloride hexahydrate (97%), iron(III) acetylacetonate (≥99.9%), cobalt(II) acetylacetonate (97%), 1,2-hexadecanediol (90%), oleic acid (90%), oleylamine (70%), benzyl ether (98%), 1-octadecene (90%) were purchased from Aldrich. Diethylene glycol (reagent) was purchased from Fisher Scientific.

Synthesis and Purification of $CoFe_2O_4$ and Fe_3O_4 Nanocrystals. $CoFe_2O_4$ nanocrystals were synthesized with modification of the recipe first reported by Sun *et al.*[11] In a typical synthesis, 8 mmol (2.8 g) iron(III) acetylacetonate, 4 mmol cobalt(II) acetylacetonate, 8 mmol (2.6 mL) oleic acid, 40 mmol (12.8 mL) oleylamine, 24 mmol (6.2 g) 1,2-hexadecanediol, and 12 mL of benzyl ether were added into a three neck flask. The mixture was first heated to 110 °C under N_2 flow and kept for 30 min, and then heated up to 205 °C and kept for 1.5 h. After that, the mixture was heated to 295 °C and held at this temperature for 1 h. The heating mantle was then removed to allow cooling. After cooling to room temperature, ethanol was added as antisolvent to precipitate $CoFe_2O_4$ nanocrystals. The precipitates were dispersed in hexane. The precipitation and dispersion were performed twice. All nanocrystals were finally dispersed in hexane.

Monodisperse Fe_3O_4 nanocrystals were synthesized by the method first reported by Hyeon *et al.*[12] First, iron oleate precursors were prepared as follows. 10.8 g of iron(III) chloride hexahydrate, 36.5 g of sodium oleate, 40 mL of DI water, 40 mL of ethanol and 80 mL of hexane were added into a three-neck flask. The mixture was heated to 60 °C and reacted for 4 h. The dark red iron oleate precursor was washed by DI water three times and dried in an oven. Second, the 12.8 nm Fe_3O_4 nanocrystals were synthesized by adding 3.6 g of iron oleate, 1 mL of oleic acid, and 20 mL of 1-octadecene into a three-neck flask. The mixture was heated up to 110 °C under N_2 flow and then heated up to 330 °C at a rate of 3 °C/min, and kept at 330 °C for 30 min. Then heating mantle was removed to allow cooling to room temperature. The 9.2 nm Fe_3O_4 nanocrystals were synthesized by adding 2 mL of oleic acid and decreasing final reaction temperature to 320 °C, while keeping all the other parameters the same. The purification of Fe_3O_4 nanocrystals is the same as above.

Self-Assembly of Binary Nanocrystal Superlattices. Large-area $CoFe_2O_4$–Fe_3O_4 BNSL membranes were obtained by the liquid–air interfacial assembly method developed by our group.[26] Briefly, a drop of hexane solution (15 μL, 5 mg/mL) containing $CoFe_2O_4$ and Fe_3O_4 nanocrystals with selected nanocrystal number ratios was drop-cast onto the surface of diethylene glycol in a Teflon well (1.5 cm × 1.5 cm × 1.5 cm), which was then covered by a glass slide. $CoFe_2O_4$–Fe_3O_4 BNSL membranes formed upon slow evaporation of hexane and were transferred from the diethylene glycol surface onto various substrates followed by vacuum drying.

Structural and Optical Characterization of Binary Nanocrystal Superlattices. BNSL films were transferred from the diethylene glycol surface to carbon-coated transmission electron microscopy (TEM) grids and SiO_2 coated TEM grids followed by vacuum drying and thermal annealing for structural characterization. TEM images and small-angle and wide-angle electron diffraction (ED) patterns were taken on a JEM-1400 transmission electron microscope equipped with a SC 1000 ORIUS CCD camera operating at 120 kV. 3D structural models were built using Materials Studio 4.4 (Accelrys Software Inc.). BNSL films were transferred from a diethylene glycol surface to double-sided polished Si wafers (5 mm × 5 mm) for Fourier-transform infrared spectra measurement. Fourier-transform infrared spectroscopy (FTIR) was carried out on a Nicolet 6700 (Thermo Fisher) spectrometer.

Thermal Annealing. Thermal annealing was carried out by rapid thermal annealing (RTA) under vacuum with base pressure of 10^{-3} Torr. BNSL films were heated from room temperature to 400 or 500 °C at heating rate of 50 °C/min and kept at 400 or 500 °C for 30 min. The sample chamber was cooled by cold circulation water. TGA was performed using a TA Instruments SDT Q600.

Magnetic Measurement of Binary Nanocrystal Superlattices. BNSL films were transferred from diethylene glycol surface to SiO_2/Si wafers (5 mm × 5 mm) followed by vacuum drying and thermal annealing. The SiO_2/Si wafers with BNSL films were then put into straws and loaded into a commercial superconducting quantum interference device (SQUID) magnetometer (Quantum Design MPMS) for magnetic measurement. The zero-field-cooled and field-cooled warming curves were taken under an applied magnetic field of 100 Oe.

Magnetoresistive Device Fabrication. Sapphire substrates were used to construct the magnetoresistive device because sapphire is a good insulator. The sapphire substrates were prepatterned by Au/Cr electrodes by thermal evaporation. The patterns of electrodes were fabricated by photolithography with 10 μm channel length and 3 mm channel width. The

self-assembled binary nanocrystal superlattice membranes floating on the diethylene glycol surface were transferred to the prepatterned sapphire substrates, dried under vacuum, and followed by thermal annealing.

Magnetotransport Measurement of Binary Nanocrystal Superlattices. The magnetotransport measurements were taken using a Keithley 237 source-measure unit in a two probe configuration, with magnetic field and temperature control provided by a Quantum Design Physical Property Measurement System (PPMS).

Conflict of Interest: The authors declare no competing financial interest.

Acknowledgment. J.C. acknowledges the support from DOE Office of ARPA-E under award DE-AR0000123. J.C., J.M.K., and C.B.M. acknowledge the MRSEC program of the National Science Foundation for support under award No. DMR 11-20901. X.Y. acknowledges the support from the Office of Naval Research (ONR) Multidisciplinary University Research Initiative (MURI) on Optical Metamaterials through award N00014-10-1-0942. S.J.O. and C.R.K. acknowledge U.S. Department of Energy Office of Basic Energy Sciences, Division of Materials Science and Engineering, under award No. DE-SC0002158. C.B.M. is also grateful to the Richard Perry University Professorship for support of his supervisor role.

Supporting Information Available: Additional structural models, TEM images, temperature dependent conductance, FC and ZFC warming curves of $CoFe_2O_4$—Fe_3O_4 BNSLs. FTIR and TGA results. Magnetization and magnetoresistance results shown up to 7 and 9 T, respectively. This material is available free of charge *via* the Internet at http://pubs.acs.org.

REFERENCES AND NOTES

1. Murray, C. B.; Kagan, C. R.; Bawendi, M. G. Synthesis and Characterization of Monodisperse Nanocrystals and Close-Packed Nanocrystal Assemblies. *Annu. Rev. Mater. Sci.* **2000**, *30*, 545–610.
2. Talapin, D. V.; Lee, J. S.; Kovalenko, M. V.; Shevchenko, E. V. Prospects of Colloidal Nanocrystals for Electronic and Optoelectronic Applications. *Chem. Rev.* **2010**, *110*, 389–458.
3. Pileni, M. P. Self-Assembly of Inorganic Nanocrystals: Fabrication and Collective Intrinsic Properties. *Acc. Chem. Res.* **2007**, *40*, 685–693.
4. Fried, T.; Shemer, G.; Markovich, G. Ordered Two-Dimensional Arrays of Ferrite Nanoparticles. *Adv. Mater.* **2001**, *13*, 1158–1161.
5. Russier, V.; Petit, C.; Legrand, J.; Pileni, M. P. Collective Magnetic Properties of Cobalt Nanocrystals Self-Assembled in a Hexagonal Network: Theoretical Model Supported by Experiments. *Phys. Rev. B* **2000**, *62*, 3910–3916.
6. Poddar, P.; Telem-Shafir, T.; Fried, T.; Markovich, G. Dipolar Interactions in Two- and Three-Dimensional Magnetic Nanoparticle Arrays. *Phys. Rev. B* **2002**, *66*, 060403.
7. Puntes, V. F.; Gorostiza, P.; Aruguete, D. M.; Bastus, N. G.; Alivisatos, A. P. Collective Behaviour in Two-Dimensional Cobalt Nanoparticle Assemblies Observed by Magnetic Force Microscopy. *Nat. Mater.* **2004**, *3*, 263–268.
8. Sun, S. H.; Murray, C. B.; Weller, D.; Folks, L.; Moser, A. Monodisperse FePt Nanoparticles and Ferromagnetic FePt Nanocrystal Superlattices. *Science* **2000**, *287*, 1989–1992.
9. Shevchenko, E. V.; Talapin, D. V.; Rogach, A. L.; Kornowski, A.; Haase, M.; Weller, H. Colloidal Synthesis and Self-Assembly of $CoPt_3$ Nanocrystals. *J. Am. Chem. Soc.* **2002**, *124*, 11480–11485.
10. Chen, M.; Nikles, D. E. Synthesis, Self-Assembly, and Magnetic Properties of $Fe_xCo_yPt_{100-x-y}$ Nanoparticles. *Nano Lett.* **2002**, *2*, 211–214.
11. Sun, S. H.; Zeng, H.; Robinson, D. B.; Raoux, S.; Rice, P. M.; Wang, S. X.; Li, G. X. Monodisperse MFe_2O_4 (M = Fe, Co, Mn) Nanoparticles. *J. Am. Chem. Soc.* **2004**, *126*, 273–279.
12. Park, J.; An, K. J.; Hwang, Y. S.; Park, J. G.; Noh, H. J.; Kim, J. Y.; Park, J. H.; Hwang, N. M.; Hyeon, T. Ultra-Large-Scale Syntheses of Monodisperse Nanocrystals. *Nat. Mater.* **2004**, *3*, 891–895.
13. Lisiecki, I.; Parker, D.; Salzemann, C.; Pileni, M. P. Face-Centered Cubic Supra-crystals and Disordered Three-Dimensional Assemblies of 7.5 nm Cobalt Nanocrystals: Influence of The Mesoscopic Ordering on The Magnetic Properties. *Chem. Mater.* **2007**, *19*, 4030–4036.
14. Ye, X. C.; Collins, J. E.; Kang, Y. J.; Chen, J.; Chen, D. T. N.; Yodh, A. G.; Murray, C. B. Morphologically Controlled Synthesis of Colloidal Upconversion Nanophosphors and Their Shape-Directed Self-Assembly. *Proc. Natl. Acad. Sci. U.S.A.* **2010**, *107*, 22430–22435.
15. Yarema, M.; Kovalenko, M. V.; Hesser, G. n.; Talapin, D. V.; Heiss, W. Highly Monodisperse Bismuth Nanoparticles and Their Three-Dimensional Superlattices. *J. Am. Chem. Soc.* **2010**, *132*, 15158–15159.
16. Ye, X. C.; Jin, L. H.; Caglayan, H.; Chen, J.; Xing, G. Z.; Zheng, C.; Vicky, D. N.; Kang, Y. J.; Engheta, N.; Kagan, C. R.; *et al.* Improved Size-Tunable Synthesis of Monodisperse Gold Nanorods through the Use of Aromatic Additives. *ACS Nano* **2012**, *6*, 2804–2817.
17. Saunders, A. E.; Korgel, B. A. Observation of an AB phase in Bidisperse Nanocrystal Superlattices. *ChemPhysChem* **2005**, *6*, 61–65.
18. Shevchenko, E. V.; Talapin, D. V.; Kotov, N. A.; O'Brien, S.; Murray, C. B. Structural Diversity in Binary Nanoparticle Superlattices. *Nature* **2006**, *439*, 55–59.
19. Chen, Z.; O'Brien, S. Structure Direction of II—VI Semiconductor Quantum Dot Binary Nanoparticle Superlattices by Tuning Radius Ratio. *ACS Nano* **2008**, *2*, 1219–1229.
20. Friedrich, H.; Gommes, C. J.; Overgaag, K.; Meeldijk, J. D.; Evers, W. H.; de Nijs, B.; Boneschanscher, M. P.; de Jongh, P. E.; Verkleij, A. J.; de Jong, K. P.; *et al.* Quantitative Structural Analysis of Binary Nanocrystal Superlattices by Electron Tomography. *Nano Lett.* **2009**, *9*, 2719–2724.
21. Smith, D. K.; Goodfellow, B.; Smilgies, D.-M.; Korgel, B. A. Self-Assembled Simple Hexagonal AB_2 Binary Nanocrystal Superlattices: SEM, GISAXS, and Defects. *J. Am. Chem. Soc.* **2009**, *131*, 3281–3290.
22. Talapin, D. V.; Shevchenko, E. V.; Bodnarchuk, M. I.; Ye, X. C.; Chen, J.; Murray, C. B. Quasicrystalline Order in Self-Assembled Binary Nanoparticle Superlattices. *Nature* **2009**, *461*, 964–967.
23. Bodnarchuk, M. I.; Kovalenko, M. V.; Heiss, W.; Talapin, D. V. Energetic and Entropic Contributions to Self-Assembly of Binary Nanocrystal Superlattices: Temperature as the Structure-Directing Factor. *J. Am. Chem. Soc.* **2010**, *132*, 11967–11977.
24. Chen, J.; Ye, X. C.; Murray, C. B. Systematic Electron Crystallographic Studies of Self-Assembled Binary Nanocrystal Superlattices. *ACS Nano* **2010**, *4*, 2374–2381.
25. Evers, W. H.; Nijs, B. D.; Filion, L.; Castillo, S.; Dijkstra, M.; Vanmaekelbergh, D. Entropy-Driven Formation of Binary Semiconductor—Nanocrystal Superlattices. *Nano Lett.* **2010**, *10*, 4235–4241.
26. Dong, A. G.; Chen, J.; Vora, P. M.; Kikkawa, J. M.; Murray, C. B. Binary Nanocrystal Superlattice Membranes Self-Assembled at the Liquid—Air Interface. *Nature* **2010**, *466*, 474–477.
27. Bodnarchuk, M. I.; Shevchenko, E. V.; Talapin, D. V. Structural Defects in Periodic and Quasicrystalline Binary Nanocrystal Superlattices. *J. Am. Chem. Soc.* **2011**, *133*, 20837–20849.
28. Dong, A.; Ye, X.; Chen, J.; Murray, C. B. Two-Dimensional Binary and Ternary Nanocrystal Superlattices: The Case of Monolayers and Bilayers. *Nano Lett.* **2011**, *11*, 1804–1809.
29. Ye, X.; Chen, J.; Murray, C. B. Polymorphism in Self-Assembled AB_6 Binary Nanocrystal Superlattices. *J. Am. Chem. Soc.* **2011**, *133*, 2613–2620.
30. Urban, J. J.; Talapin, D. V.; Shevchenko, E. V.; Kagan, C. R.; Murray, C. B. Synergism in Binary Nanocrystal Superlattices Leads to Enhanced p-Type Conductivity in Self-Assembled PbTe/Ag_2Te Thin Films. *Nat. Mater.* **2007**, *6*, 115–121.
31. Shevchenko, E. V.; Ringler, M.; Schwemer, A.; Talapin, D. V.; Klar, T. A.; Rogach, A. L.; Feldmann, J.; Alivisatos, A. P. Self-Assembled Binary Superlattices of CdSe and Au Nanocrystals and Their Fluorescence Properties. *J. Am. Chem. Soc.* **2008**, *130*, 3274–3275.

32. Chen, J.; Dong, A.; Cai, J.; Ye, X.; Kang, Y.; Kikkawa, J. M.; Murray, C. B. Collective Dipolar Interactions in Self-Assembled Magnetic Binary Nanocrystal Superlattice Membranes. *Nano Lett.* **2010**, *10*, 5103–5108.
33. Dong, A.; Chen, J.; Ye, X.; Kikkawa, J. M.; Murray, C. B. Enhanced Thermal Stability and Magnetic Properties in NaCl-Type FePt-MnO Binary Nanocrystal Superlattices. *J. Am. Chem. Soc.* **2011**, *133*, 13296–13299.
34. Kneller, E. F.; Hawig, R. The Exchange-Spring Magnet—A New Material Principle for Permanent Magnets. *IEEE Trans. Magn.* **1991**, *27*, 3588–3600.
35. Zeng, H.; Li, J.; Wang, Z. L.; Liu, J. P.; Sun, S. H. Bimagnetic core/shell FePt/Fe_3O_4 Nanoparticles. *Nano Lett.* **2004**, *4*, 187–190.
36. Zeng, H.; Sun, S. H.; Li, J.; Wang, Z. L.; Liu, J. P. Tailoring Magnetic Properties of Core/Shell Nanoparticles. *Appl. Phys. Lett.* **2004**, *85*, 792–794.
37. Kang, S. S.; Miao, G. X.; Shi, S.; Jia, Z.; Nikles, D. E.; Harrell, J. W. Enhanced Magnetic Properties of Self-Assembled FePt Nanoparticles with MnO Shell. *J. Am. Chem. Soc.* **2006**, *128*, 1042–1043.
38. Bodnarchuk, M. I.; Kovalenko, M. V.; Groiss, H.; Resel, R.; Reissner, M.; Hesser, G.; Lechner, R. T.; Steiner, W.; Schaffler, F.; Heiss, W. Exchange-Coupled Bimagnetic Wustite/Metal Ferrite Core/Shell Nanocrystals: Size, Shape, and Compositional Control. *Small* **2009**, *5*, 2247–2252.
39. Casavola, M.; Falqui, A.; Garcia, M. A.; Garcia-Hernandez, M.; Giannini, C.; Cingolani, R.; Cozzoli, P. D. Exchange-Coupled Bimagnetic Cobalt/Iron Oxide Branched Nanocrystal Heterostructures. *Nano Lett.* **2009**, *9*, 366–376.
40. Lee, J.-H.; Jang, J.-t.; Choi, J.-s.; Moon, S. H.; Noh, S.-h.; Kim, J.-w.; Kim, J.-G.; Kim, I.-S.; Park, K. I.; Cheon, J. Exchange-Coupled Magnetic Nanoparticles for Efficient Heat Induction. *Nat. Nanotechnol.* **2011**, *6*, 418–422.
41. Song, Q.; Zhang, Z. J. Controlled Synthesis and Magnetic Properties of Bimagnetic Spinel Ferrite $CoFe_2O_4$ and $MnFe_2O_4$ Nanocrystals with Core—Shell Architecture. *J. Am. Chem. Soc.* **2012**, *134*, 10182–10190.
42. Zeng, H.; Li, J.; Liu, J. P.; Wang, Z. L.; Sun, S. H. Exchange-Coupled Nanocomposite Magnets by Nanoparticle Self-Assembly. *Nature* **2002**, *420*, 395–398.
43. Zeng, H.; Black, C. T.; Sandstrom, R. L.; Rice, P. M.; Murray, C. B.; Sun, S. H. Magnetotransport of Magnetite Nanoparticle Arrays. *Phys. Rev. B* **2006**, *73*, 020402.
44. Jang, S. J.; Kong, W. J.; Zeng, H. Magnetotransport in Fe_3O_4 Nanoparticle Arrays Dominated by Noncollinear Surface Spins. *Phys. Rev. B* **2007**, *76*, 212403.
45. Taub, N.; Tsukernik, A.; Markovich, G. Inter-Particle Spin-Polarized Tunneling in Arrays of Magnetite Nanocrystals. *J. Magn. Magn. Mater.* **2009**, *321*, 1933–1938.
46. Ramos, A. V.; Matzen, S.; Moussy, J.-B.; Ott, F.; eacute, ric; Viret, M. Artificial Antiphase Boundary at the Interface of Ferrimagnetic Spinel Bilayers. *Phys. Rev. B* **2009**, *79*, 014401.
47. Black, C. T.; Murray, C. B.; Sandstrom, R. L.; Sun, S. H. pin-Dependent Tunneling in Self-Assembled Cobalt-Nanocrystal Superlattices. *Science* **2000**, *290*, 1131–1134.
48. Xiao, J. Q.; Jiang, J. S.; Chien, C. L. Giant Magnetoresistance in Nonmultilayer Magnetic Systems. *Phys. Rev. Lett.* **1992**, *68*, 3749–3752.